80 Gb/s OAM-PDM-OQPSK FSO system under extensive weather conditions-performance analysis

NAGA SUBRAHMANYA VAMSI MOHAN YARRA[1,*], SIVANANTHA RAJA A.[1], ESAKKI MUTHU K.[2]
[1]*Department of Electronics and Communication Engineering, Alagappa Chettiar Government College of Engineering and Technology, Karaikudi, Tamilnadu, India*
[2]*Department of Electronics and Communication Engineering, University VOC College of Engineering, Thoothukudi, Tamilnadu, India*

This research paper investigates free space optic (FSO) system by integrating orbital angular momentum (OAM) and polarization division multiplexing (PDM) techniques resulting in the data rate enhancement. Simulation of OAM-PDM-FSO transmission is analyzed by using Optisystem. A successful transmission of 80 Gb/s overall capacity is investigated by means of individual OAM modes ($LG_{0,0}$, $LG_{0,13}$, $LG_{0,40}$, and $LG_{0,80}$), enhancing the spectral efficiency of the system under different climatic conditions. System performance is studied for various modulation schemes including return-to-zero (RZ), non-return-to zero (NRZ) and offset-quadrature-phase shift keying (OQPSK). The best performance has been shown by means of OQPSK modulation technique. 8x10 Gb/s transmission under the influence of various external weather conditions such as rain, fog and dust is reported. A maximum FSO link range of 6 km is realized under clear weather conditions whereas a maximum FSO range of 0.125 km is achieved under heavy dust conditions. A satisfactory Bit Error rate (BER) < 10^{-6} and eye diagrams with wider opening heights for all eight channels achieved. The FSO system also achieves satisfactory BER for various turbulence levels. Performance of proposed hybrid OAM-PDM system is evaluated at different link lengths in terms of Q-factor, log (BER), received power and eye diagrams.

(Received May 8, 2023; accepted October 9, 2023)

Keywords: OAM, FSO, OQPSK, MDM, Laguerre Gaussian modes

1. Introduction

The continuously evolving multimedia applications need increased wireless potential of 5th generation (5G) [1]. The requirements of 5G including virtual reality, fast connectivity and the internet of things (IoT) are supposed to be met by making use of huge bandwidths available in millimeter wave bands [2]. 5G is expected to quench bandwidth hungry applications and also to enable the IoT [3]. Ultra dense deployment of micro cells in comparison to macro cells is supposed to be a key technique for the 5G networks [4]. A. Ijaz et al. [5] published a design for IoT provision in 5G systems to enable massive IoT in 5G. Optical wireless communication (OWC) technology, which is complementary to its radio frequency (RF) counterpart, displayed its ability to support huge traffic generated by connectivity of IoT and 5G systems [6]. The 5G radio access network (RAN) system which is expected to be a wireless web world-wide connects everything, supports 1000-times traffic, 100 billion devices, and quality of service (QoS) requirements of multimedia applications by the year 2020 [7].

On account of 5G, control as well as data planes separation architecture has been conceived as an interesting paradigm that has ability to tackle most of challenges that arrive with network densification [8].

M. R. Palattella et al. illustrated [9] the enormous business shifts that a link between IoT and 5G could cause in the operator and vendors' ecosystem. One technology that could help to cope with new data services and applications that are emerging is OWC [10].

FSO, which is one of the different technologies of OWC, suffers from atmospheric turbulence caused by scintillation effect. The main impaired factors to accomplish an optical link are atmospheric conditions like dust, fog and rain etc. These atmospheric conditions affect visibility. They result in absorption of the light beam, causing power attenuation. These external factors increase the path loss which is analyzed in the form of BER of FSO link.

Mode division multiplexing (MDM) is a novel technique in which Eigen modes are used to transmit simultaneously independent information streams over distinct spatial modes [11]. Eigen modes can enhance the capacity of FSO. Eigen modes are used for the propagation of a number of channels on different modes generated by various approaches such as spatial light modulators, optical signal processing, photonic crystal fibers, modal decomposition methods and few-mode fiber [12]. MDM can enhance bandwidth, which is used for enhancing the capacity of FSO networks. The spectral bandwidth of FSO can further be increased by integrating PDM with MDM where PDM uses dual polarization (X and Y-polarizations) to carry signals [13]. MDM is preferred when compared to other multiplexing techniques such as WDM because it is much economical and uses a single laser source [14]. Wavelength-division-multiplexing (WDM) and Optical time division multiplexing (OTDM) are examples of

parallel transmission. To increase the number of parallel channels, MDM technique is used. MDM is popular because of high data rate carrying capacity. It is used in FSO to boost the system capacity. OAM is one of the variants of MDM. Due to the high number of modes that can be used in a single optical channel, MDM transmission is of significant interest. Spatial laser modes in MDM are utilized as independent channels that will carry various data streams. By transmitting various independent data streams in parallel mode, MDM technique permits the capacity of a communication system to be increased. This simultaneous transmission of information on OAM modes is possible due to the orthogonality property of OAM beams that allows transmission without interference between signals [15]. MDM can be used to increase the transportation data rate by a quantity proportional to the number of modes [16]. MDM is a multiplexing technique that optimizes spectrum efficiency and data rates. It extends the transmission range in FSO systems at acceptable SNR.

Multiple studies proposed the implementation of Laguerre–Gaussian (LG) and Hermite Gaussian (HG) modes [17] in FSO systems employing multiple channels under high attenuation environments such as dense dust/ fog and heavy rain weather conditions. One of the techniques used for transmitting information is to encode a distinct data stream on each OAM mode, multiplex among the other modes, and transmit along the transmission medium. Data can be mapped also onto advanced modulation formats such as quadrature-phase-shift-keying (QPSK) and quadrature-amplitude-modulation (QAM) [18]. OAM beams for multiplexing can be considered as similar to several other multiplexing technologies which can be used to enhance the total transmission capacity, communication range and spectral efficiency. Examples are wavelength division multiplexing (WDM), time division multiplexing (TDM), space division multiplexing (SDM), polarization division multiplexing (PDM) and mode-division multiplexing (MDM). OAM multiplexing can be combined, with other multiplexing techniques such as wavelength division multiplexing (WDM), orthogonal code division multiple access (OCDMA) [19], polarization division multiplexing (PDM) and orthogonal frequency-division multiplexing (OFDM) [20]. Section 2 discusses the OAM based FSO system architecture, and Section 3 explains system performance under atmospheric attenuation. Section 4 discusses the results and finally Section 5 concludes this research paper.

2. OAM -based FSO system architecture

Fig. 1 and Fig. 2 show the Transmitter and Receiver blocks of OAM based FSO system architecture respectively.

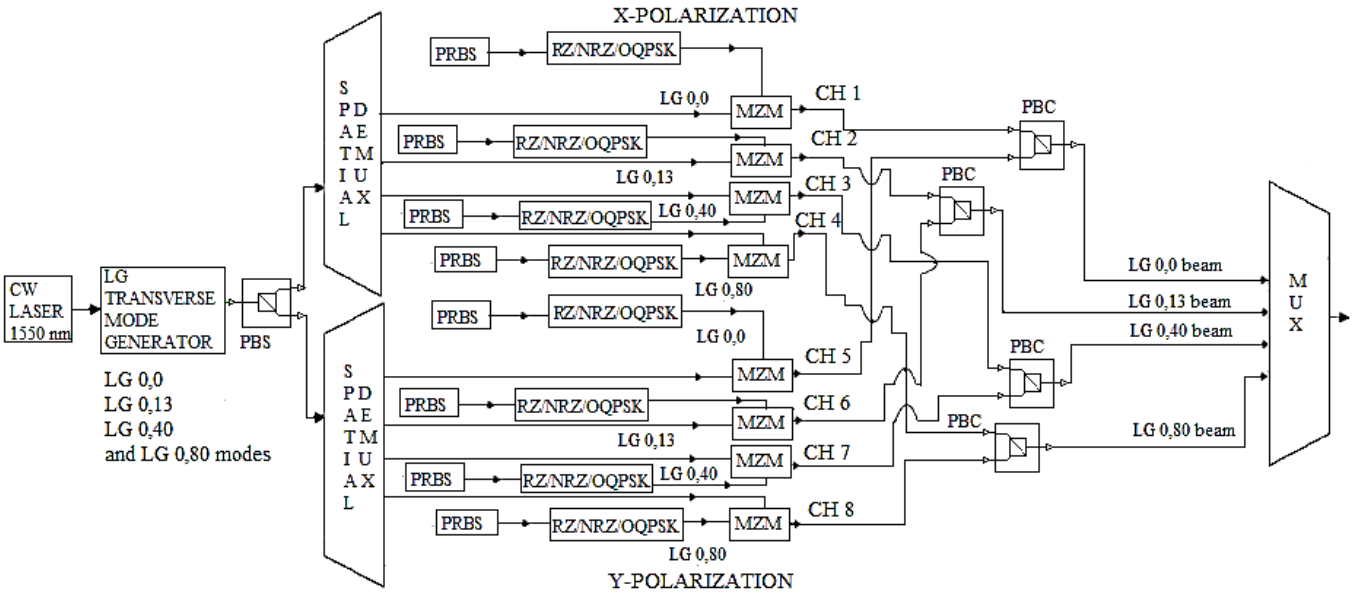

Fig. 1. Transmitter Block

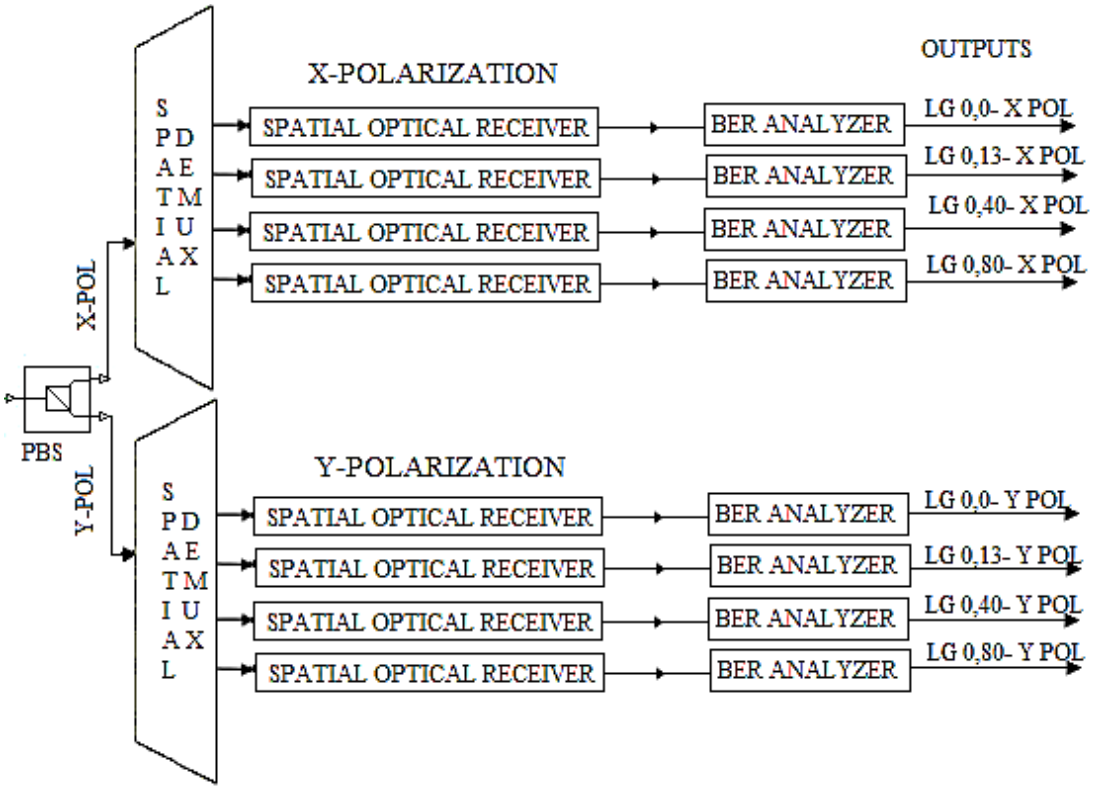

Fig. 2. Receiver Block (X-POL/Y-POL indicates X-Polarization and Y-Polarization respectively)

Spatial distribution of LG modes can be expressed [21] as

$$u(r,\phi,z) = \sqrt{\frac{2p!}{\pi(p+|m|)!}}\frac{1}{\omega(z)}\left[\frac{r\sqrt{2}}{\omega(z)}\right]^{|m|} L_{p,m}\left[\frac{2r^2}{\omega^2(z)}\right] \times \exp\left[\frac{-r^2}{\omega^2(z)}\right]\exp\left[\frac{-ikr^2z}{2Z^2+2{Z_R}^2}\right] \times \exp\left[i(2p+|m|+1)\tan^{-1}\frac{z}{Z_R}\right]\exp(-im\phi) \quad (1)$$

where ϕ and r indicate the angular and the radial coordinates, $\omega(z)$ denotes the waist size of the light beam at link distance z, z_R indicates the Rayleigh range, $k=2\pi/\lambda$ indicates the wave-number expressed in radians per meter and λ denotes the optical signal wavelength.

$L_{p,m}$ indicates the Laguerre Gaussian polynomial where p and m denote the mode indices in the radial and azimuthal directions respectively. OAM beams can be modulated individually for the propagation of multiple data streams. Dual polarization of four independent OAM modes$LG_{0,0}$, $LG_{0,13}$, $LG_{0,40}$, and $LG_{0,80}$ are made to transmit independent 10 Gb/s binary data over free-space communication channel.

CW laser, together with LG transverse mode generator produces four Laguerre Gaussian OAM modes $LG_{0,0}$, $LG_{0,13}$, $LG_{0,40}$, and $LG_{0,80}$. At the transmitter side, output of LG transverse mode generator splits through dual-polarization (X-Polarization and Y-Polarization) by means of polarization beam splitter (PBS). Each of these X and Y polarization signals are then divided into four different LG modes by means of two spatial de-multiplexers. These four LG modes are applied to four Mach-Zehnder modulators (MZM). Four Pseudo random bit sequence (PRBS) generators which generate random bit sequence for RZ/NRZ/OQPSK at the data rate of 10 Gb/s and further applied to RZ/NRZ/OQPSK pulse generators. These RZ/NRZ/OQPSK pulse generators are fed to MZM's which give the optical modulated signals. Then, the same modes of these two different polarized signals are combined in the polarization beam combiners (PBC) and these signals are sent into the multiplexer. This 80Gb/s multiplexed signal is transmitted over the FSO channel.

On receiver side, the polarization beam splitter (PBS) detects the polarization state. Spatial de-multiplexers split the corresponding individual OAM modes. The respective modes get detected by means of spatial optical receivers. The spatial optical receivers convert the optical signals back into electrical form. Hence eight outputs are produced for the entire FSO system. The proposed system has the ability to transmit 80 Gbits/s [1-wavelength×2-polarization states × 4-LG modes × 10 Gbits/s] of data. Fig. 3 shows 2D- top views of various excited LG modes.

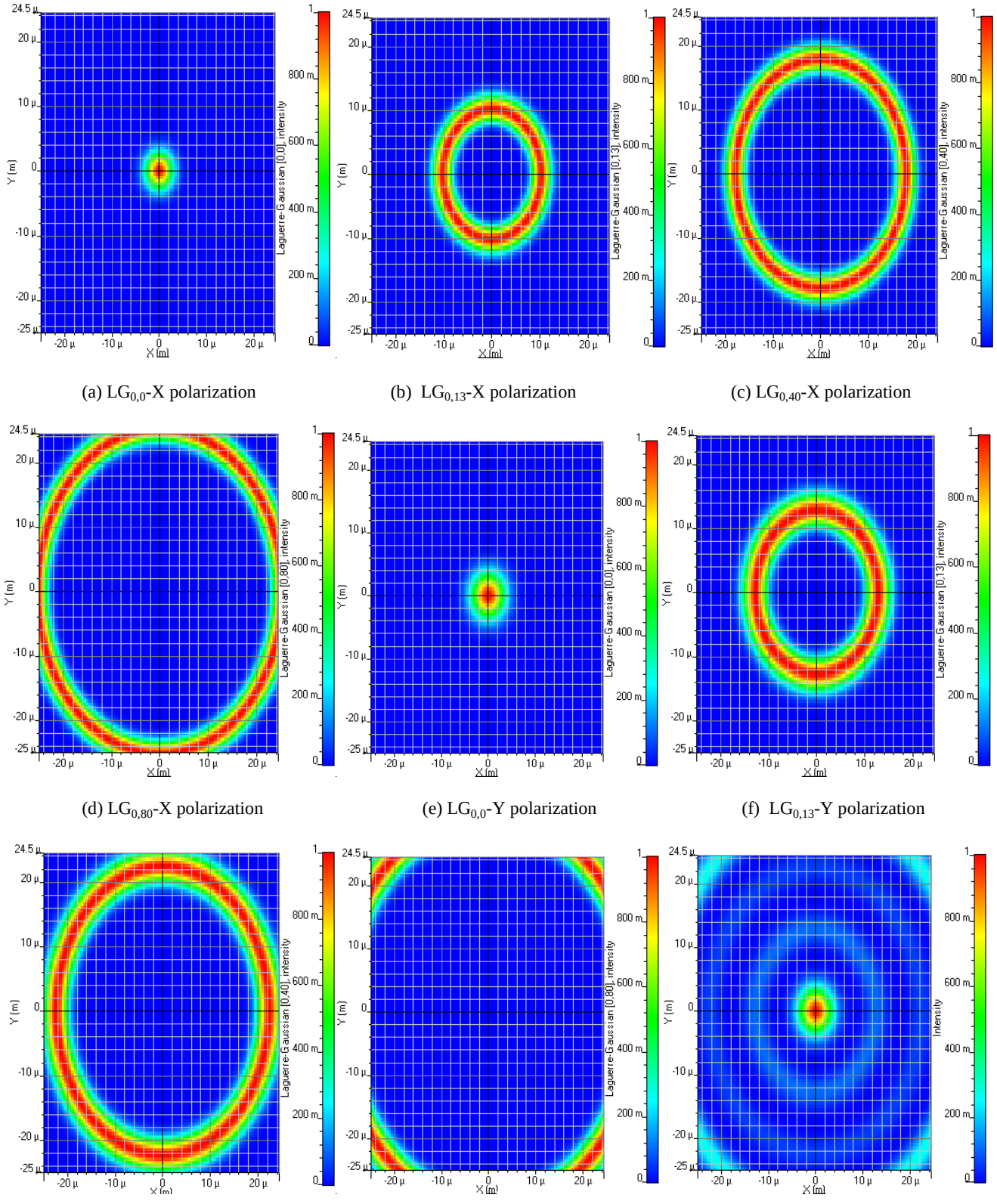

(a) $LG_{0,0}$-X polarization (b) $LG_{0,13}$-X polarization (c) $LG_{0,40}$-X polarization

(d) $LG_{0,80}$-X polarization (e) $LG_{0,0}$-Y polarization (f) $LG_{0,13}$-Y polarization

(g) $LG_{0,40}$-Y polarization (h) $LG_{0,80}$-Y polarization (i) OAM multiplexed signal at the receiver side

Fig. 3. 2D- top views of excited LG modes:(a) $LG_{0,0}$ – X polarization (b) $LG_{0,13}$– X polarization(c) $LG_{0,40}$ – X polarization (d) $LG_{0,80}$– X polarization(e) $LG_{0,0}$ – Y polarization (f) $LG_{0,13}$– Y polarization (g) $LG_{0,40}$ – Y polarization(h) $LG_{0,80}$– Y polarization (i) OAM multiplexed signal at the receiver (color online)

Table 1. System parameters that are considered for the research work [19]

Parameter	Values
Data rate	10 Gbps
CW laser frequency	193.1 THz
CW laser power	30 dBm
OAM beams	$LG_{0,0}$, $LG_{0,13}$, $LG_{0,40}$ and $LG_{0,80}$
Sequence length	2048
Samples per bit	64
Samples considered	131072
Wavelength	1550 nm
Transmitter aperture diameter	5 cm
Receiver aperture diameter	20 cm
Divergence angle	1.5 mrad
Laser spectral width	10 MHz
PIN responsivity	1 A/W
Dark current	10 nA
Electrical bandwidth	0.75 x Symbol rate
Modulation schemes used	RZ, NRZ and OQPSK
Clear weather (CW) attenuation	0.14 dB/km
Attenuation for LF, MF, and DF	9, 16 and22 dB/km, respectively
Attenuation for LR, MR, and DR	6.27, 9.64, and 19.28 dB/km, respectively
Attenuation for LD, MD, and DD	25.11, 107.11, and 297.38 dB/km, respectively
Turbulence model used	Gamma- Gamma model

LF/LR/LD indicates low fog/rain/dust respectively. MF/MR/MD indicates moderate fog/rain/dust respectively and DF/DR/DD indicates dense (high) fog/rain/dust respectively.

Table 1 displays values of the system parameters that are used in the simulation of the proposed FSO system. The received optical signal power in terms of the transmitted power P_t for the FSO system [22] is given by

$$P_r = P_t \left[\frac{{d_r}^2}{(d_t + \Theta R)^2}\right] (\tau_t \tau_r)_{X\,10} - \alpha R/10 \qquad (2)$$

where d_r and d_t are the receiver and transmitter aperture diameters respectively, Θ is the beam divergence, $\mathbf{R}$ is the FSO link length, α is the atmospheric attenuation factor, τ_t and τ_r are transmitter and receiver optical efficiencies respectively. The performance of the hybrid OAM-PDM multiplexed FSO system transmission has been investigated for different weather conditions. For the analysis of the effects of various environmental conditions on FSO link, the attenuation of the channel has been made as variable. The measured log (BER) in terms of FSO link range for channel 1 to channel 8 for RZ, NRZ and OQPSK modulation formats has been displayed in Fig. 4. The log (BER) value increases with an increase in the FSO link distance for various schemes. The lowest BER value has been achieved in case of OQPSK modulation scheme. OQPSK shows superior performance among the three modulation schemes. Hence OQPSK modulation scheme has been selected for further performance analysis of the FSO system considering various environmental conditions. The OQPSK modulation is a PSK modulation. This modulation scheme uses two bits per symbol and one bit delay in the quadrature signal. For OQPSK scheme, symbol rate is half the bit rate. It occupies half the bandwidth compared to BPSK waveform. Hence available bandwidth is more effectively utilized. OQPSK de-modulated signal provides a flexible hardware platform used in wireless communications where high data rate transportation is needed such as satellite communication [23, 24]. OQPSK is more suited compared to QPSK in mobile communication since the performance of OQPSK is better than the performance of QPSK when both the schemes have the same parameters [25]. H.Alifdal et al. [26] reported that using OQPSK modulation can improve system performance.

Table 2 shows the log (BER), Q-factor and received power values for clear weather when FSO link range is 6 km for channel 1 to channel 8 respectively for OQPSK modulation scheme.

Table 2. Log (BER), Q-factor and received power for clear weather when the FSO range = 6 km for 8 channels (OQPSK)

Polarization	Channels	Log (BER)	Q-factor	Received power (dBm)
X-Polarization	1	-8.26	5.68	-17.05
	2	-8.67	5.85	-17.06
	3	-8.06	5.60	-17.09
	4	-8.47	5.77	-17.06
Y-Polarization	5	-8.26	5.68	-17.05
	6	-8.67	5.85	-17.06
	7	-8.06	5.60	-17.09
	8	-8.47	5.77	-17.06

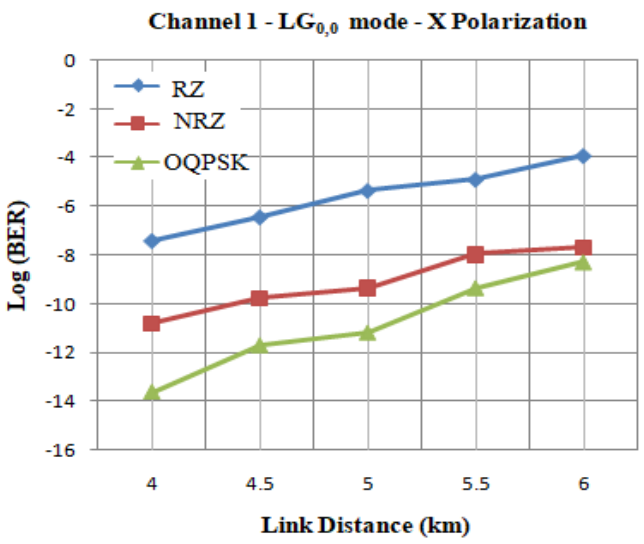

(a) Channel 1- $LG_{0,0}$ mode – X Polarization

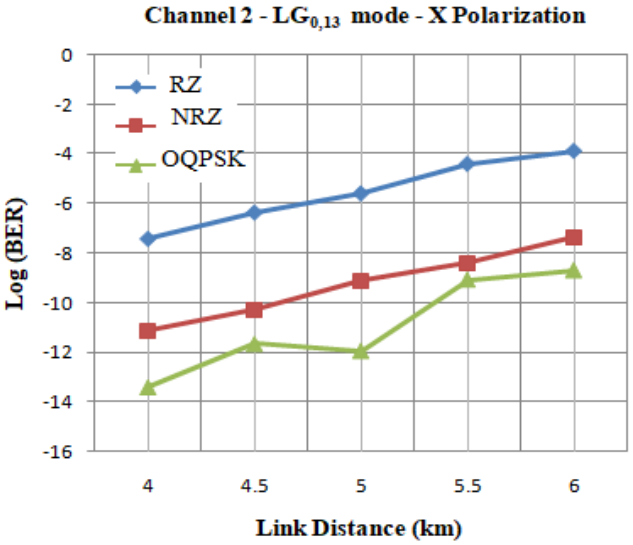

(b) Channel 2- $LG_{0,13}$ mode – X Polarization

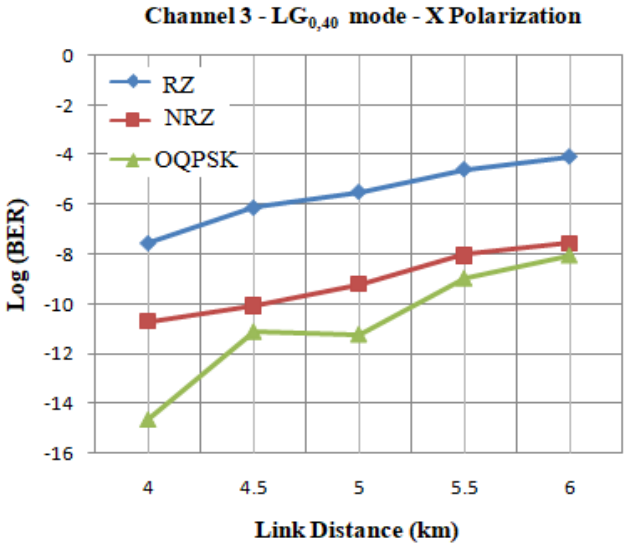

(c) Channel 3- $LG_{0,40}$ mode – X Polarization

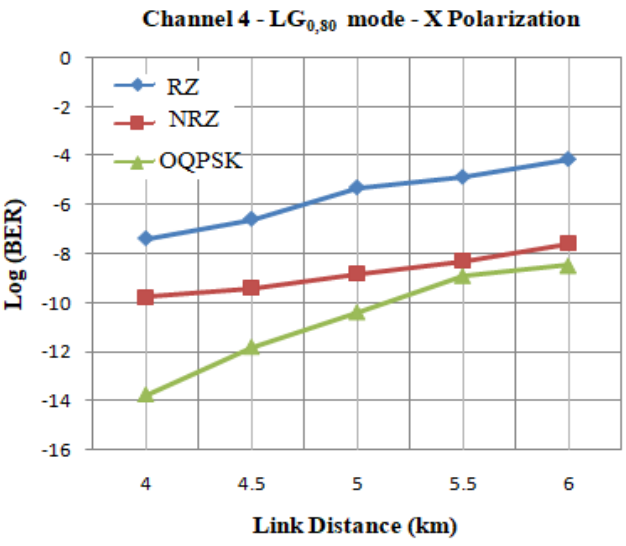

(d) Channel 4- $LG_{0,80}$ mode – X Polarization

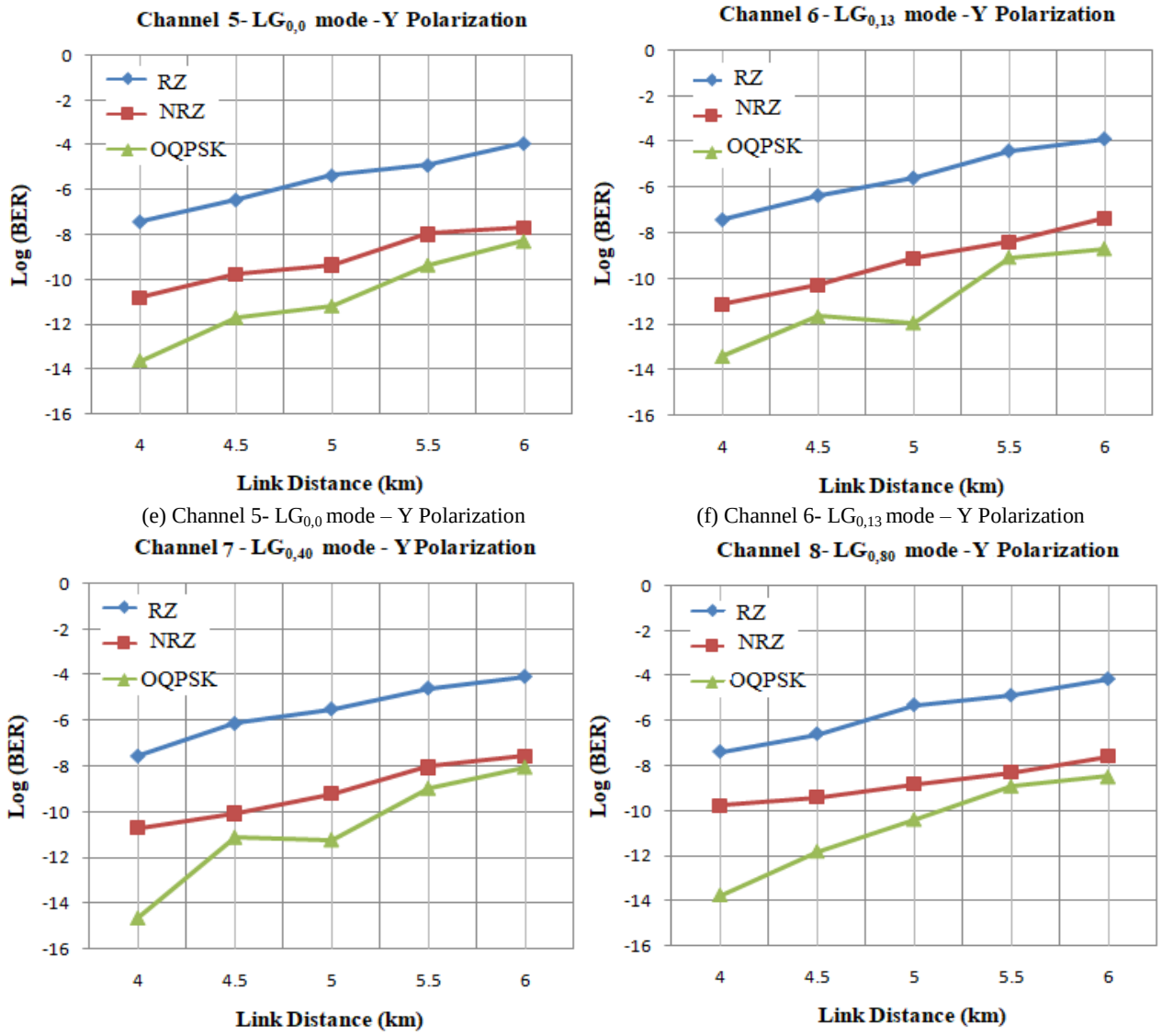

(e) Channel 5- $LG_{0,0}$ mode – Y Polarization

(f) Channel 6- $LG_{0,13}$ mode – Y Polarization

(g) Channel 7- $LG_{0,40}$ mode – Y Polarization

(h) Channel 8- $LG_{0,80}$ mode – Y Polarization

Fig. 4. Log(BER) vs Link distance (km) under clear weather conditions for RZ, NRZ and OQPSK (color online)

3. System performance under atmospheric attenuation

The adverse effects of atmospheric channel such as absorption, scattering and fading due to atmospheric turbulence cause attenuation, so that the performance of the FSO communication link deteriorates [27]. Absorption is wavelength dependent which occurs while optical beams come in contact with atmospheric suspended particles in free space. Fog, dust and rain absorb the light beam, resulting in attenuation of light power. Scattering is a wavelength dependent process [28]. The communication link range gets affected by the attenuation. Fog is one environmental condition by which absorption as well as scattering of light beam takes place. The accurate estimation for attenuation of fog/mist can be done by means of applying Mie scattering theory. The attenuation coefficient [29] for fog is given by

$$\beta_{\text{fog/mist}} = \frac{3.91}{V}\left[\frac{\lambda}{550}\right]^{-q} \quad (3)$$

Here V is the visibility range expressed in km, λ is the wavelength measured in nm and q indicates the size distribution coefficient of the scattering particles. One more crucial environmental condition that limits the FSO transmission link range is rain. Rain causes wavelength-independent scattering. The specific attenuation for rain [28, 30] can be modeled by Marshal and Palmer model and is given as

$$\beta_{\text{rain}} = 0.365R^{0.63} \quad (4)$$

Here R is the rain rate in mm/hr. Dust causes absorption of power by dust particles present in atmosphere and wavelength dependent scattering. The wavelength dependent specific attenuation [31] for dust is given by

$$\beta_{\text{dust}} = 52V^{-1.05} \quad (5)$$

4. Results and discussion

The measured log (BER) in terms of FSO link range for Channel 1, OQPSK modulation format has been displayed in Fig. 5 for different intensities of rain. Table 3 shows log (BER), Q-factor and received power for Channel 1 (OAM beam $LG_{0,0}$-X-Pol) under rain.

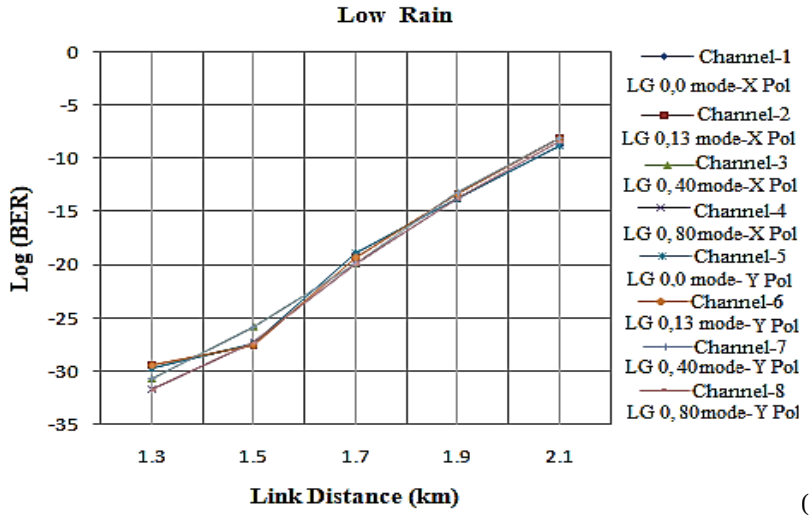

(a) Low rain

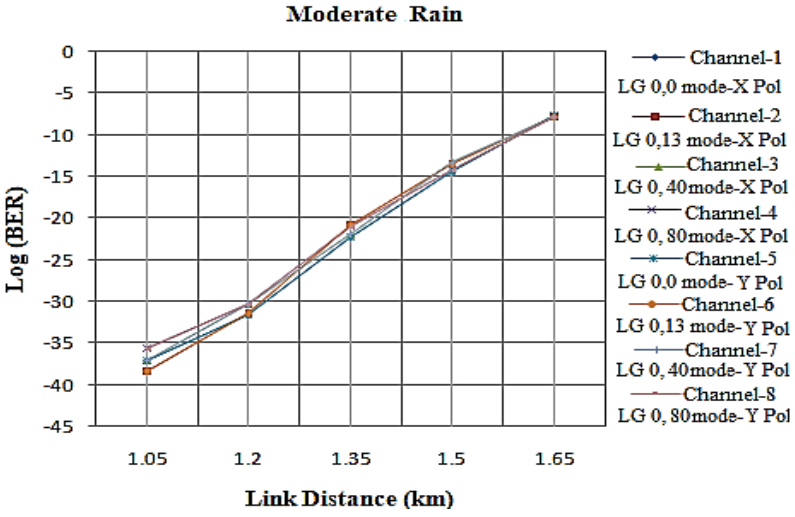

(b) Moderate rain

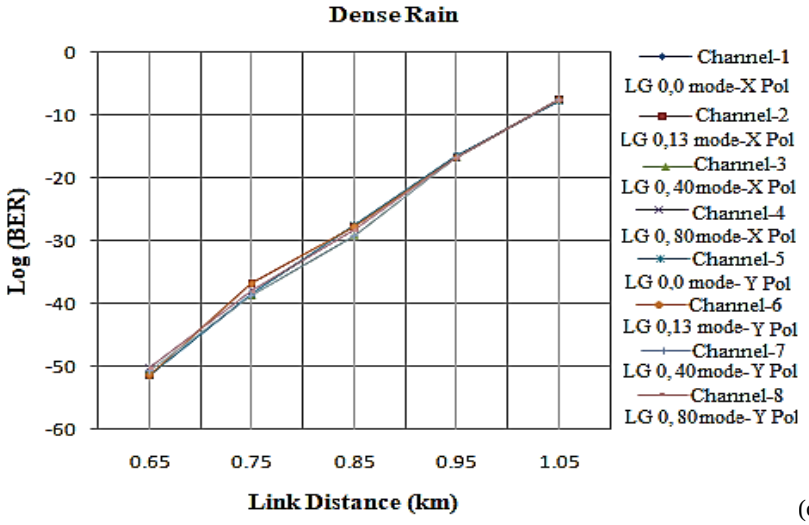

(c) Dense rain

Fig. 5. Log (BER) vs Link distance (km) under different rain conditions (color online)

Table 3. Log (BER), Q-factor and received power values for Channel 1 (OAM beam $LG_{0,0}$-X-Pol) under rain conditions

Parameters	LR (2.1 km)	MR (1.65 km)	DR (1.05 km)
Log (BER)	-8.74	-7.69	-7.64
Q-factor	5.89	5.49	5.47
Received power (dBm)	-19.73	-20.32	-20.7

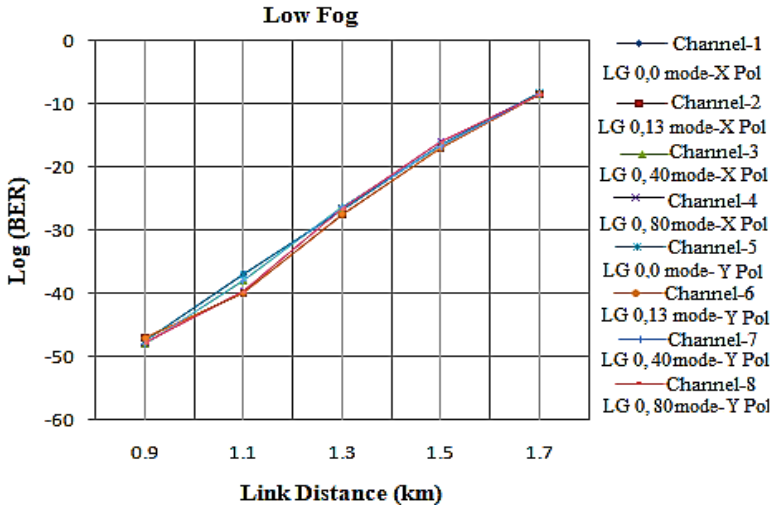

(a) Low fog

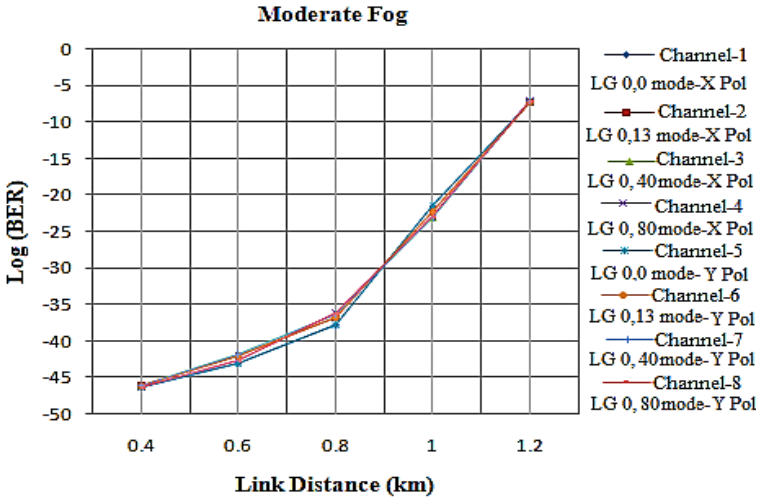

(b) Moderate fog

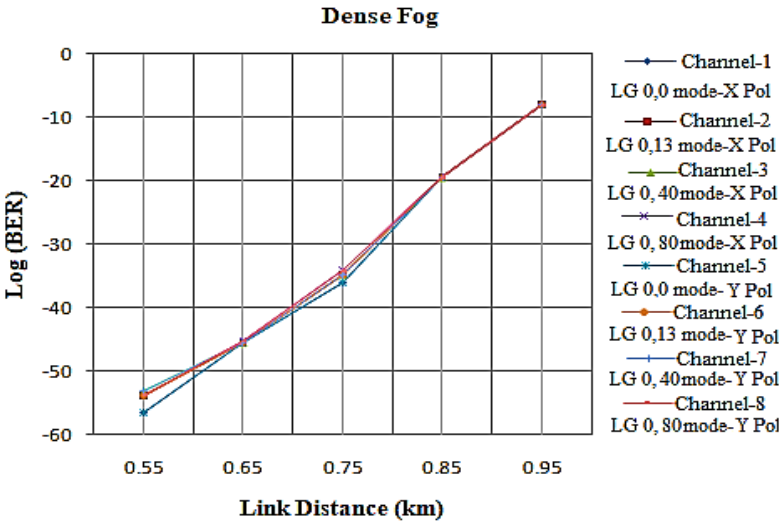

(c) Dense fog

Fig. 6. Log (BER) vs Link distance (km) under different fog conditions (color online)

Table 4. Log (BER), Q-factor and received power values for Channel 1 (OAM beam $LG_{0,0}$-X-Pol) under fog conditions using OQPSK modulation scheme

Parameters	LF (1.7 km)	MF (1.2 km)	DF (0.95 km)
Log (BER)	-8.33	-7.22	-7.95
Q-factor	5.74	5.29	5.59
Received power (dBm)	-19.97	-20.81	-20.49

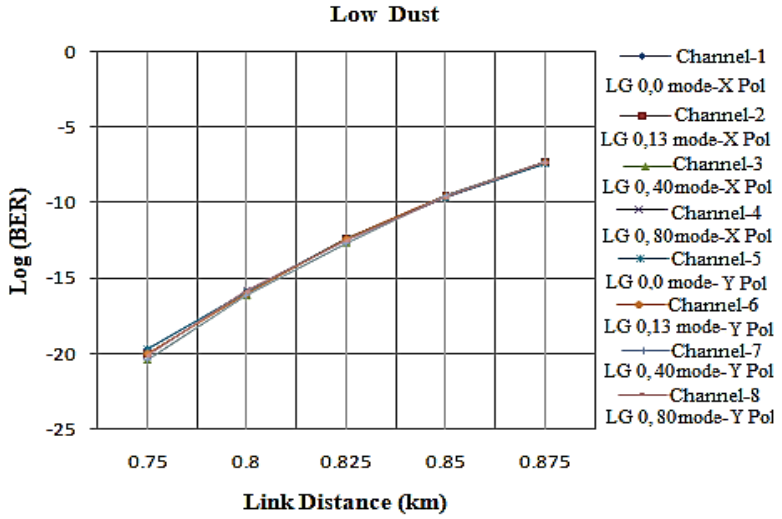

(a) Low dust

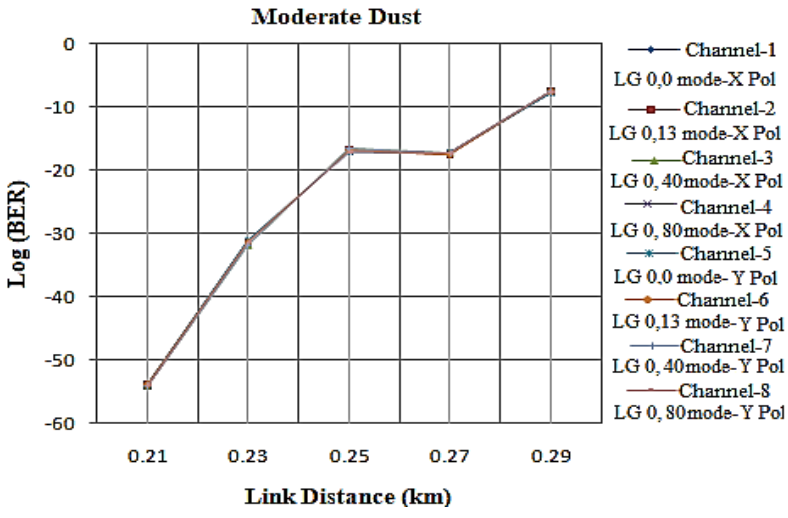

(b) Moderate dust

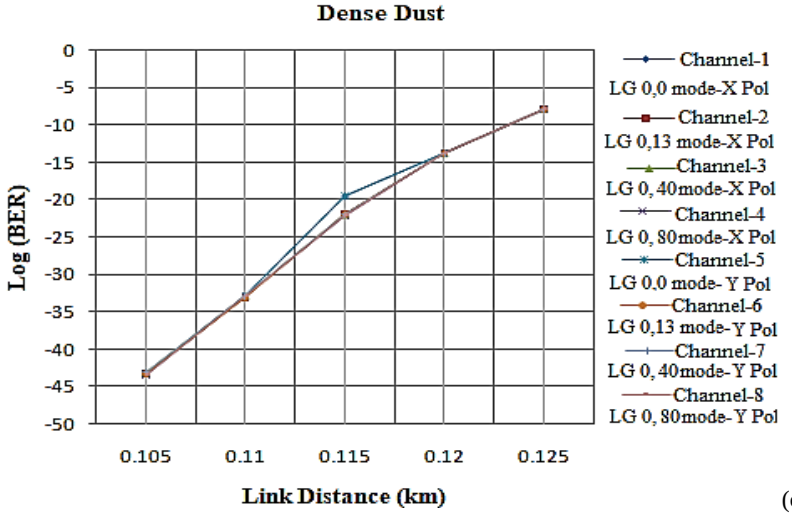

(c) Dense dust

Fig. 7. Log (BER) vs Link distance (km) under different dust conditions (color online)

The measured log (BER) in terms of FSO link range for channel 1, OQPSK modulation format has been displayed in Fig. 6 for different intensities of fog. Table 4 shows log (BER), Q-factor and received power values for Channel 1 (OAM beam $LG_{0,0}$-X-Pol) under fog. The measured log (BER) in terms of FSO link range for channel 1, OQPSK modulation format has been displayed in Fig. 7 for different intensities of dust. Table 5 shows log (BER), Q-factor and received power values for Channel 1 (OAM beam $LG_{0,0}$-X-Pol) under dust.

Table 5. Log (BER), Q-factor and received power values for Channel 1 (OAM beam $LG_{0,0}$-X-Pol) under dust conditions using OQPSK modulation scheme

Parameters	LD (0.875 km)	MD (0.29 km)	DD (0.125 km)
Log (BER)	-7.41	-7.66	-7.79
Q-factor	5.37	5.47	5.53
Received power (dBm)	-20.86	-20.91	-20.81

Due to atmospheric turbulence, the refractive index of a wireless medium fluctuates. Hence the transmitted signal gets attenuated. This randomness is expressed as the index refraction structure (C_n^2). Rytov proposed atmospheric turbulence loss [32] as

$$\sigma^2 = 1.23 C_n^2 \left(\frac{2\pi}{\lambda}\right)^{\frac{7}{6}} (L)^{\frac{11}{6}} \quad (6)$$

Here σ^2 is the Rytov variance, L is the link distance and C_n^2 is the index refraction structure.

Fig. 8 shows the log (BER) versus C_n^2 curve for weak turbulence ($C_n^2 = 5 \times 10^{-17}$ $m^{-2/3}$), moderate turbulence ($C_n^2 = 5 \times 10^{-15}$ $m^{-2/3}$) and strong turbulence ($C_n^2 = 5 \times 10^{-13}$ $m^{-2/3}$) conditions at different weather scenarios. A satisfactory BER level is achieved for low turbulence level and medium turbulence levels. Once the turbulence level increases, the FSO communication system performance reduces.

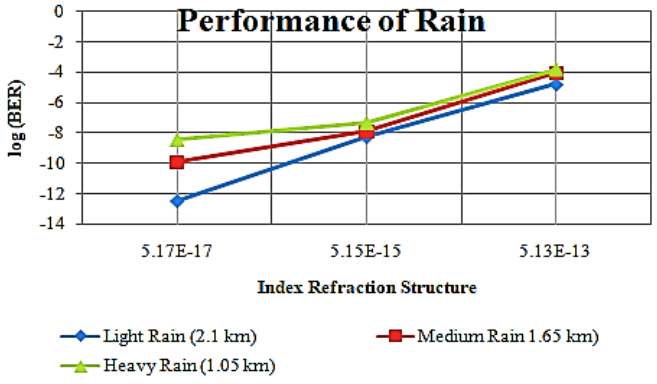

(a) Performance of Rain

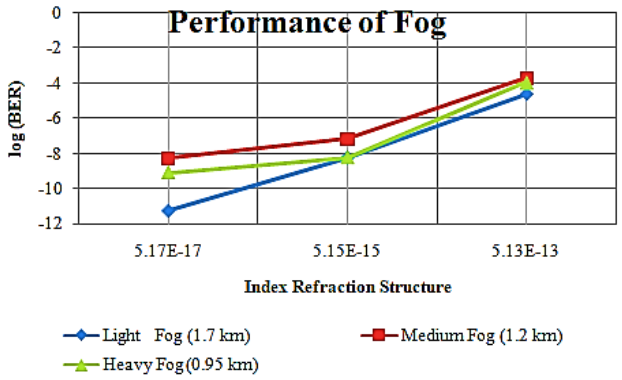

(b) Performance of Fog

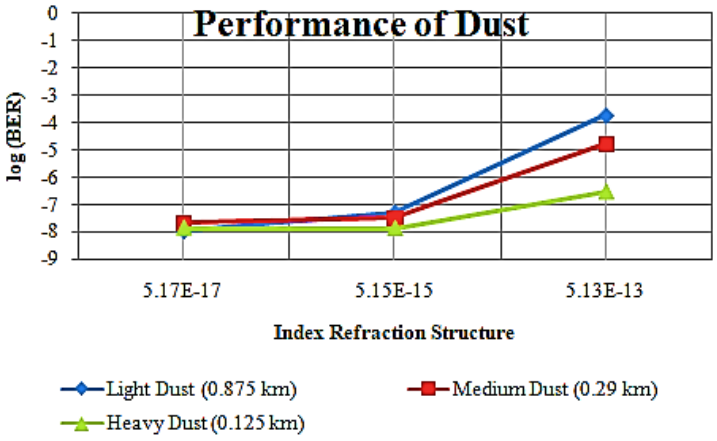

(c) Performance of Dust

Fig. 8. Log (BER) vs Index refraction structure under different atmospheric turbulence levels (color online)

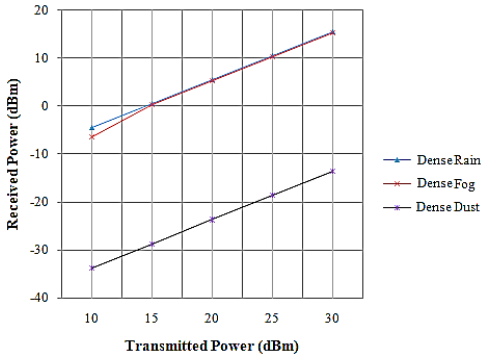

Fig. 9. Received power vs transmitted power under different weather conditions (color online)

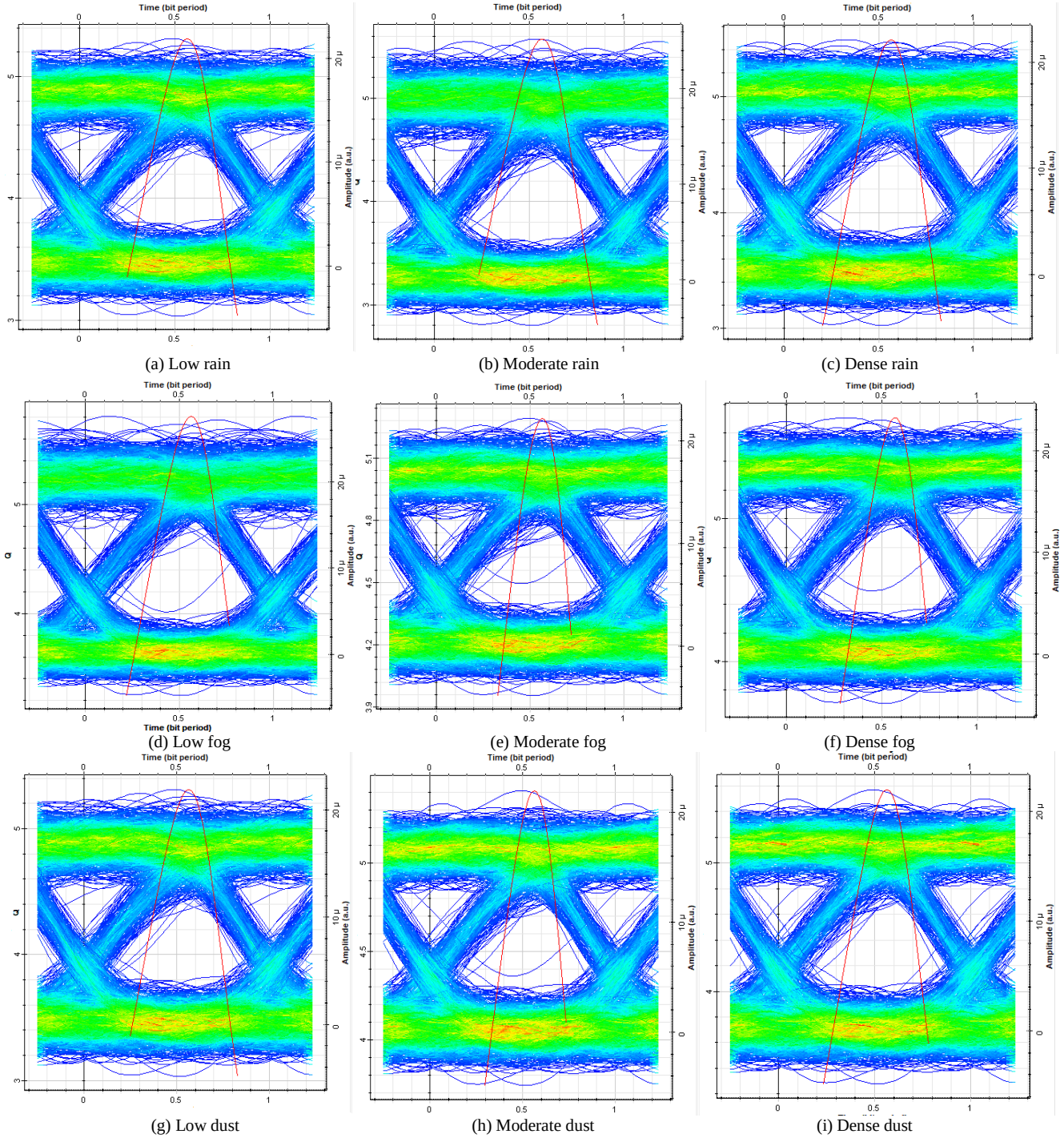

(a) Low rain (b) Moderate rain (c) Dense rain

(d) Low fog (e) Moderate fog (f) Dense fog

(g) Low dust (h) Moderate dust (i) Dense dust

Fig. 10. Eye diagrams of Channel 1 (LG $_{0,0}$) for low/moderate/dense- rain, fog and dust (color online)

The graphs between the received power and the transmitted power under the impact of various environmental conditions such as dense rain, dense fog and dense dust for various values of transmitted power from 10 to 30 dBm considering $LG_{0,0}$ mode are displayed in Fig. 9. The received power increases with increase in the transmitted power. Highest received power occurs under the conditions of rain and lowest received power occurs under the influence of dust out of the three weather conditions of rain, fog and dust. When the power transmitted is 30 dBm, the received power values are 15.51 dBm, 15.23 dBm and -13.69 dBm for dense rain, dense fog and dense dust respectively when a link distance of 0.105 km is considered.

Fig. 10 shows the eye diagrams for the Channel 1 ($LG_{0,0}$) under different atmospheric conditions such as rain, fog and dust. All the eye diagrams show wider eye opening heights, which indicate successful FSO transmission. Table 6 shows a comparison of results for the proposed research work with existing work.

Table 6. Comparison of results for the proposed research work with existing work

Author/ Work	Modulation Scheme/ Multiplexing Technique	Capacity/each Channel	Total Capacity	Weather conditions/ Max link distance (km)
M. Singh et al. [33]	4 OAM beams NRZ	10 Gbps	4x10 Gbps	CW: 0.80 LH: 0.65 MH: 0.575 HH: 0.45 LR: 0.51 MR: 0.45 HR: 0.35 LF: 0.48 MF: 0.375 HF: 0.32
M. Singh et al. [34]	OCDMA PDM EDW code	10 Gbps	2x3x10 Gbps	CW: 4.0 LH: 2.6 MH: 1.8 HH: 1.16 LR: 1.15 MR: 1.18 HR: 0.76 LF: 1.22 MF: 0.86 HF: 0.68
M. Singh et al. [35]	OCDMA 4 OAM beams EDW code	10 Gbps	4x3x10 Gbps	CW: 0.28 LH: 0.23 MH: 0.205 HH: 0.18 LR: 0.195 MR: 0.185 HR: 0.145 LF: 0.187 MF: 0.16 HF: 0.135
S. Chaudhary et al. [36]	PDM-OCDMA RD code	10 Gbps	10x10 Gbps	LF: 1.8 MF: 1.3 HF: 1.0
M. Singh et al. [37]	OFDM-OCDMA EDW code	15 Gbps	3x15 Gbps	CW: 3.450 LF: 1.085 MF: 0.784

				HF: 0.645 LD: 0.681 MD: 0.232 HD: 0.102
Proposed Research	4 OAM beams PDM OQPSK	10 Gbps	4x2x10 Gbps	CW: 6.00 LR: 2.10 MR: 1.65 HR: 1.05 LF: 1.70 MF: 1.20 HF: 0.95 LD: 0.875 MD: 0.29 HD: 0.125

5. Conclusion

The research article shows that the proposed FSO transmission system performs better as compared to the previous works by incorporating hybrid OAM and PDM techniques. An aggregate data rate equal to 80 Gbps is achieved. Hence, there is an improvement in data rate of 8 times. The maximum FSO transmission distances vary from 0.125 km to 6 km based on various types of weather conditions, atmospheric attenuation, and turbulence levels. A satisfactory BER < 10^{-6} and eye diagrams with wider opening heights for all eight channels achieved. The FSO system also achieves satisfactory BER for various turbulence levels. Results indicate that due to improvement in system performance, high data rate transportation, and more effective utilization of the available bandwidth, OQPSK is found out to be the best modulation technique when compared with NRZ and RZ. Future work to investigate other multiplexing techniques such as orthogonal frequency division multiplexing (OFDM) and optical code division multiple access (OCDMA) can be considered.

References

[1] M. Z. Chowdhury, M. T. Hossan, A. Islam, Y. M. Jang, IEEE Access **6**, 9819 (2018).

[2] M. Shafi, A. F. Molisch, P. J. Smith, T. Haustein, P. Zhu, P. De Silva, F. Tufvesson, A. Benjebbour, G. Wunder, IEEE Journal on Selected Areas in Communications **35**(6), 1201 (2017).

[3] M. Jaber, M. A. Imran, R. Tafazolli, A. Tukmanov, IEEE Access **4**, 1743 (2016).

[4] U. Siddique, H. Tabassum, E. Hossain, D. Kim, IEEE Wireless Communications **22**(5), 22 (2015).

[5] A. Ijaz, L. Zhang, M. Grau, A. Mohamed, S. Vural, A. U. Quddus, M. A. Imran, C. H. Foh, R. Tafazolli, IEEE Access **4**, 3322 (2016).

[6] M. Z. Chowdhury, M. K. Hasan, M. Shahjalal, M. T. Hossan, Y. M. Jang, IEEE Communications Surveys and Tutorials **22**(2), Second Quart. 930 (2020).

[7] T. O. Olwal, K. Djouani, A. M. Kurien, IEEE Communications Surveys and Tutorials **18**(3), Third Quart. 1656 (2016).

[8] H. A. U. Mustafa, M. A. Imran, M. Z. Shakir, A. Imran, R. Tafazolli, IEEE Communications Surveys and Tutorials **18**(1), First Quart. 419 (2016).

[9] M. R. Palattella, M. Dohler, A. Grieco, G. Rizzo, J. Torsner, T. Engel, L. Ladid, IEEE Journal on Selected Areas in Communications **34**(3), 510 (2016).

[10] Z. Ghassemlooy, S. Arnon, M. Uysal, Z. Xu, J. Cheng, IEEE Journal on Selected Areas in Communications **33**(9), 1738 (2015).

[11] A. Grover, A. Sheetal, V. Dhasarathan, Wireless Netw. **26**, 343 (2020).

[12] R. Murad, A. Amphawan, Y. Fazea, M. Sajat, H. Alias, Proceeding of International Conference on Electrical Engineering, Computer Science and Informatics, **TW-08**, 117 (2015).

[13] S. Chaudhary, L. Wuttisittikulkij, J. Nebhen, X. Tang, M. Saadi, S. Al Otaibi, A. Althobaiti, A. Sharma, S. Choudhary, Front. Phys. **9**, 756232 (2021).

[14] Y. Wang, Y. Chen, Y. Zhang, H. Y. Chen, S. Yu, Journal of Optics **18**(5), 1 (2016).

[15] E. M. Amhoud, B. S. Ooi, M. S. Alouini, IEEE Transactions on Wireless Communications. **19**(2), 888 (2020).

[16] G. Milione, M. P. J. Lavery, H. Huang, Y. Ren, G. Xie, T. A. Nguyen, E. Karimi, L. Marrucci, D. A. Nolan, R. R. Alfano, A. E. Willner, Opt. Lett. **40**, 1980 (2015).

[17] M. Singh, A. Grover, M. Kumari, A. Sheetal, R. Sharma, Suvidhi, Optoelectron. Adv. Mat. **16**(3-4), 121 (2022).

[18] A. Trichili, K. H. Park, M. Zghal, B. S. Ooi, M. S. Alouini, IEEE Communication Surveys and Tutorials **21**(4), 3175 (2019).

[19] M. Singh, M. H. Aly, S. A. A. El-Mottaleb, Appl. Opt. **62**, 142 (2023).

[20] T. Hu, Y. Wang, X. Liao, J. Zhang, Q. Song, IEEE

Access **7**, 59114 (2019).
[21] G. R. Mehrpoor, M. Safari, B. Schmauss, 4th International Workshop on Optical Wireless Communications (IWOW) 7342270, 78 (2015).
[22] M. Singh, S. Bhatia, H. Kaushal, Proceedings of the Second International Conference on Computer and Communication Technologies, Advances in intelligent systems and computing, Springer, New Delhi **379**, 329 (2016).
[23] S. Parkash, A. Banga, D. Kumar, International Journal of Engineering Applied Sciences and Technology **7**(9), 147 (2022).
[24] P. Zicari, E. Sciagura, S. Perri, P. Corsonello, Microprocessors and Microsystems **32**(8), 437 (2008).
[25] M. Tan, S. He, W. Song, H. Liu, Z. Liu, W. Fang, 6th International Conference on Wireless Communications Networking and Mobile Computing (WiCOM) 5600117, 1 (2010).
[26] H. Alifdal, F. Abdi, F. M. Abbou, International Conference on Wireless Technologies, Embedded and Intelligent Systems (WITS) 40758, 1 (2017).
[27] R. Rani, G. Kaur, 7th International Conference on Signal Processing and Communication (ICSC) 9673278, 31 (2021).
[28] H. Kaushal, G. Kaddoum, IEEE Communications Surveys and Tutorials **19**(1), First quarter 57 (2017).
[29] Z. Ghassemlooy, W. Popoola, S. A. Fares, F. Adachi, Intech Open, Rijeka, ISBN978-953-307-042, 355 (2010).
[30] J. S. Marshall, W. M. Palmer, J. J. Meteorol. **5** (4), 165 (1948).
[31] M. Singh, S. N. Pottoo, J. Malhotra, A. Grover, M. H. Aly, Alexandria Engineering Journal **60**(5), 4275 (2021).
[32] J. Mohale, M. R. Handura, T. O. Olwal, C. N. Nyirenda, Optical Engineering **55**, 1 (2016).
[33] M. Singh, A. Atieh, A. Grover, O. Barukab, Alexandria Eng. J. **61**(7), 5203 (2022).
[34] M. Singh, M. H. Aly, S. A. A. El-Mottaleb, Optik **264** 169415 (2022).
[35] M. Singh, A. Atieh, M. H. Aly, S. A. A. El-Mottaleb, Alexandria Engineering Journal **61**(12), 10407 (2022).
[36] S. Chaudhary, A. Sharma, X. Tang, X. Wei, P. Sood, Wireless Personal Commun. **116**, 2159 (2020).
[37] M. Singh, J. Kríž, M. M. Kamruzzaman, V. Dhasarathan, A. Sharma, S. A. A. El-Mottaleb, Frontiers in Physics **10**, 934848 (2022).

*Corresponding author: Anuragh2468@gmail.com